ELSEVIER

Volume 207 November 2013 ISSN 0022-4596

JOURNAL OF SOLID STATE CHEMISTRY

IN THIS ISSUE:

$Na_8Au_{9.8(4)}Ga_{7.2}$ and $Na_{17}Au_{5.87(2)}Ga_{46.63}$: The diversity of pseudo 5-fold symmetries in the Na–Au–Ga system

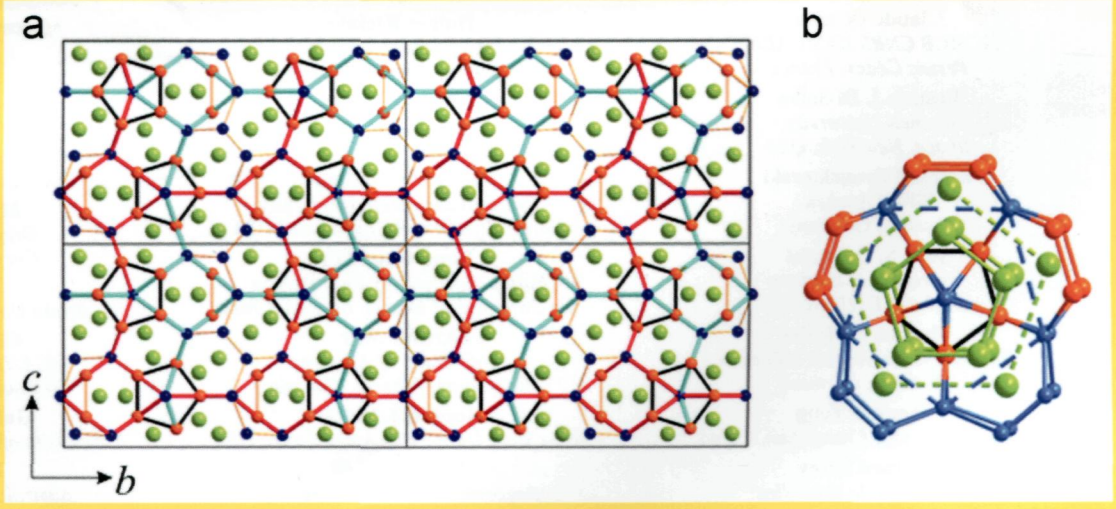

Volodymyr Smetana, John D. Corbett and Gordon J. Miller

Available online at www.sciencedirect.com

ScienceDirect

ELSEVIER

Volume 207, November 2013

JOURNAL OF SOLID STATE CHEMISTRY

www.elsevier.com/locate/jssc

CONTENTS

Abstracted/indexed in BioEngineering Abstracts, Chemical Abstracts, Coal Abstracts, Current Contents/Physics, Chemical, & Earth Sciences, Engineering Index, Research Alert, SCISEARCH, Science Abstracts, and Science Citation Index. Also covered in the abstract and citation database SCOPUS®. Full text available on ScienceDirect®.

Regular Articles

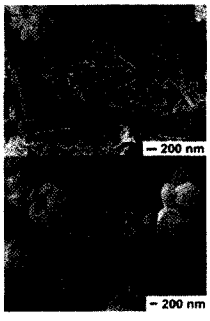

SEM images of the ZrB2-SiC powders obtained by different methods.

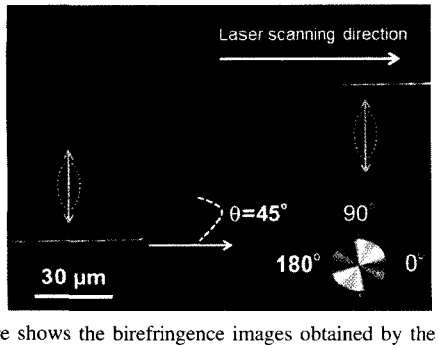

This figure shows the birefringence images obtained by the Abrio IM imaging system (λ=546 nm) for the laser-patterned β-BaB_2O_4 crystal line with the bending angle of 45° in the glass. The relation between the direction of slow axis and color is also shown. It is demonstrated that the formation (crystallization) of highly *c*-axis oriented β-BaB_2O_4 crystals follows along laser scanning direction even if the laser scanning direction changes.

Regular Articles—Continued

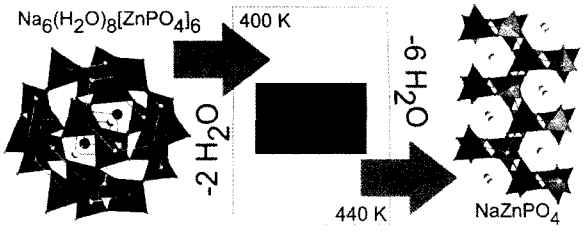

The thermal decomposition of $|Na_6(H_2O)_8|[ZnPO_4]_6$ sodalite is a two-step process with an initial loss of two water molecules at 400 K, intermediately stabilizing the highly stressed framework. Further heating leads to a subsequent loss of the remaining six water molecules and a breakup of the sodalite framework. A beryllonite-type $NaZnPO_4$ is the final product of this process.

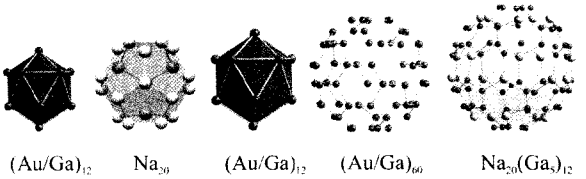

Multiply-endohedral Bergman-related clusters in the structure of $Na_{17}Au_{5.9(1)}Ga_{46.6}$.

Continued

Molecular dynamics studies of the size and temperature dependence of the kinetics of freezing of Fe nanoparticles
Bo Zhao, Jinfan Huang and Lawrence S. Bartell
page 35

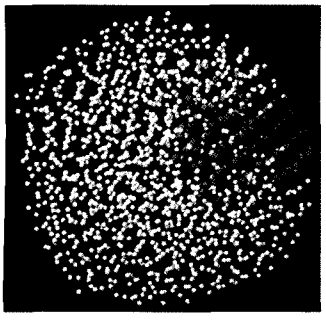

Critical nuclei of crystallization.

Two-dimensional titanium carbonitrides and their hydroxylated derivatives: Structural, electronic properties and stability of *MX*enes $Ti_3C_{2-x}N_x(OH)_2$ from DFTB calculations
A.N. Enyashin and A.L. Ivanovskii
page 42

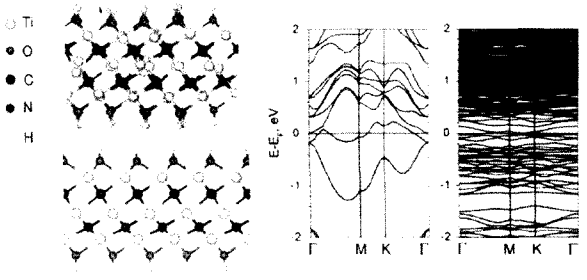

The side views of the optimized atomic structures of some examined hydroxylated derivatives of *MX*ene Ti_3CN and their electronic band structures.

Luminescence properties of a blue-emitting phosphor: $(Sr_{1-x}Eu_x)Si_9Al_{19}ON_{31}$ ($0<x\leq1$)
Lihong Liu, Rong-Jun Xie, Naoto Hirosaki, Benjamin Dierre and Takashi Sekiguchi
page 49

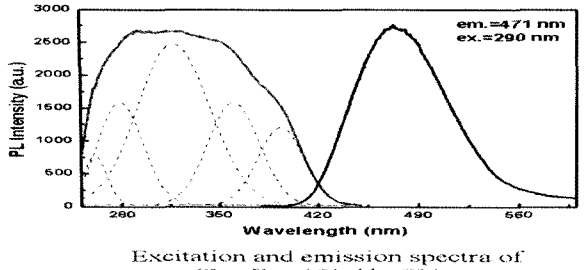

Excitation and emission spectra of $(Sr_{0.7}Eu_{0.3})Si_9Al_{19}ON_{31}$

$Sr_{0.7}Eu_{0.3}Si_9Al_{19}ON_{31}$ gives blue-emitting at 471 nm. Excitation spectrum is composed of five bands in the range of 250–450 nm, which are matching well with emission wavelength of UV LEDs.

$BaZn_2Si_2O_7$ and the solid solution series $BaZn_{2-x}Co_xSi_2O_7$ ($0<x\leq2$) as high temperature seals for solid oxide fuel cells studied by high-temperature X-ray diffraction and dilatometry
Marita Kerstan, Christian Thieme, Matthias Grosch, Matthias Müller and Christian Rüssel
page 55

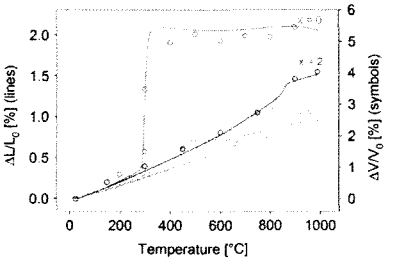

The composition of the solid solution $BaZn_{2-x}Co_xSi_2O_7$ strongly affects the thermal expansion.

1D coordination polymers formed by tetranuclear lead(II) building blocks with carboxylate ligands: In situ isomerization of itaconic acid
Abhinandan Rana, Swapan Kumar Jana, Sayanti Datta, Raymond J. Butcher, Ennio Zangrando and Sudipta Dalai
page 61

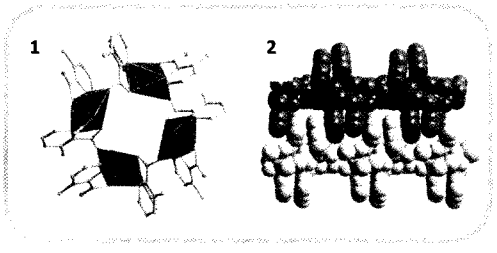

Two new topologically different 1D coordination polymers formed by Pb_4 clusters have been synthesized and characterized by X-ray analysis. The luminescence and thermal properties have been studied.

Synthesis and structural and magnetic characterization of the frustrated magnetic system $La_2Ni_{4/3-x}Co_xSb_{2/3}O_6$
D.G. Franco, R.E. Carbonio and G. Nieva
page 69

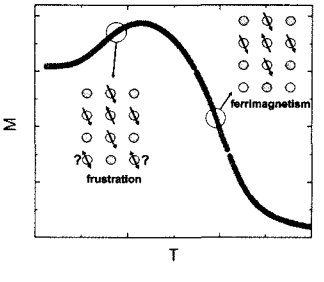

Luminescence of erbium ions in tellurite glasses
Alexander P. Savikin, Igor A. Grishin, Valery V. Sharkov and Andrei V. Budruev
page 80

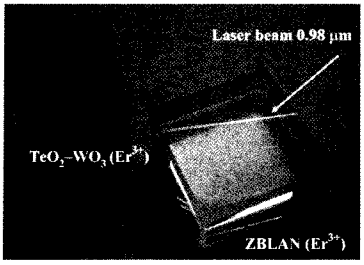

In contrast to the case of ZBLAN glass the TeO_2–WO_3 (Er^{3+}) glass has bright intensity of luminescence at 1.53 μm for erbium ions that should be caused by excitation at 975 nm. Experimental data obtained have shown the possibility to use the studied glasses doped by Er^{3+} and Yb^{3+} as active elements for fiber and integrated optics.

Interaction of yttrium with nickel and phosphorus: Phase diagram and structural chemistry
Olga Zhak, Stanislav Stoyko, Volodymyr Babizhetskyy, Olena Shved, Stepan Oryshchyn and Constantin Hoch
page 87

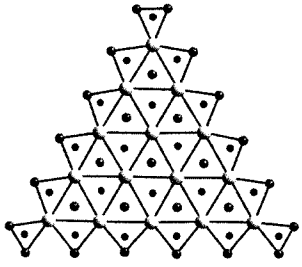

Structure block with the composition $Ln_{10}M_{21}X_{15}$ of the homologous series of the compounds $(Ln,M)_{-2}X$.

Simultaneous presence of $(Si_3O_{10})^{8-}$ and $(Si_2O_7)^{6-}$ groups in new synthetic mixed sorosilicates: $BaY_4(Si_2O_7)(Si_3O_{10})$ and isotypic compounds, studied by single-crystal X-ray diffraction, Raman spectroscopy and DFT calculations
Maria Wierzbicka-Wieczorek, Daniel M. Többens, Uwe Kolitsch and Ekkehart Tillmanns
page 94

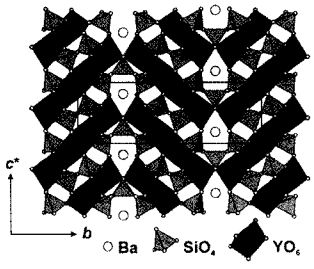

View of $BaY_4(Si_2O_7)(Si_3O_{10})$ along [100], showing zigzag chains and the tri- and disilicate groups. The unit cell is outlined.

A new member of "114" family $Ca_{1-x}Eu_xBaZn_{2+x}Ga_{2-x}O_7$ ($x \leq 0.24$): Structure and luminescence
Pengfei Jiang, Zexi Liu, Xiaorui Sun, Wenliang Gao, Rihong Cong and Tao Yang
page 105

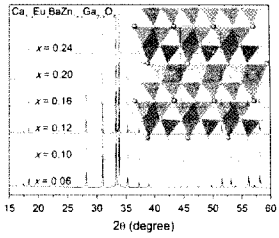

Reitveld refinements show $Ca_{1-x}Eu_xBaZn_{2+x}Ga_{2-x}O_7$ all crystallize in $P6_3mc$. By Eu^{3+}-doping, O3 show the most obvious movement (~0.08 Å) along the c-axis.

Crystal and magnetic structure of $(1-x)BiFeO_3$–$xSrTiO_3$ (x=0.2, 0.3, 0.4 and 0.8)
D.J. Goossens, C.J. Weekes, Maxim Avdeev and W.D. Hutchison
page 111

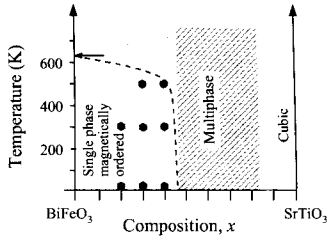

A simple phase diagram for $(1-x)BiFeO_3$–$xSrTiO_3$, where hexagons indicate the rhombohedral $R3c$ phase and boxes the cubic phase. Filled symbols indicate magnetic ordering. The black arrow indicates T_N for $BiFeO_3$.

Investigation of the hydrothermal crystallisation of the perovskite solid solution $NaCe_{1-x}La_xTi_2O_6$ and its defect chemistry
Mohammad H. Harunsani, David I. Woodward, Martin D. Peel, Sharon E. Ashbrook and Richard I. Walton
page 117

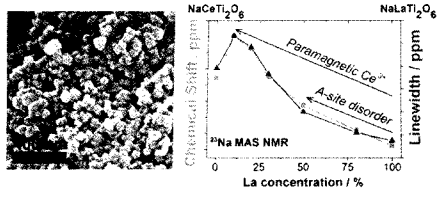

A multi-element A-site perovskite crystallises directly from aqueous, basic solutions at 240 °C; while the paramagnetic effect of Ce^{3+} on the ^{23}Na NMR shows a homogeneous solid-solution, the incorporation of A-site water is also found from ^2H NMR and IR, with oxidation of some cerium to charge balance proved by XANES spectroscopy.

Continued

Synthesis, magnetic and electric transport properties of mixed-valence manganites $La_{0.5+x}Sr_{1.5-x}Mn_{0.5}Cr_{0.5}O_4$ (x=0.1, 0.2 and 0.3)

Devinder Singh and Arun Mahajan

page 126

Unit cell structure of $La_{0.6}Sr_{1.4}Mn_{0.5}Cr_{0.5}O_4$.

Hydrothermal reactions: From the synthesis of ligand to new lanthanide 3D-coordination polymers

Fausthon Fred da Silva, Carlos Alberto Fernandes de Oliveira, Eduardo Henrique Lago Falcão, Claudia Cristina Gatto, Nivan Bezerra da Costa Jr., Ricardo Oliveira Freire, Jarosław Chojnacki and Severino Alves Júnior

page 132

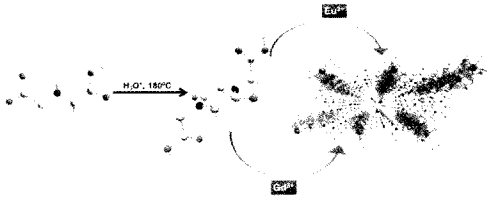

Scheme of obtaining the ligand 2,5-piperazinedione-1,4-diacetic acid (H_2PDA) and two new isostructural 3D-coordination polymers $[Ln(PDA)_{1.5}(H_2O)](H_2O)_3$ (Ln=Gd^{3+} and Eu^{3+}) by hydrothermal synthesis.

Ab initio density functional theory investigation of the structural, electronic and optical properties of Ca_3Sb_2 in hexagonal and cubic phases

Borhan Arghavani Nia, Matin Sedighi, Masoud Shahrokhi and Rostam Moradian

page 140

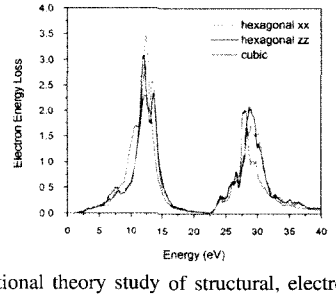

A density functional theory study of structural, electronic and optical properties of Ca_3Sb_2 compound in hexagonal and cubic phases is presented.

Three-dimensional assemblies built up by quantum dots in size-quantization regime: Band gap shifts due to size-distribution of cadmium selenide nanoparticles

Biljana Pejova

page 147

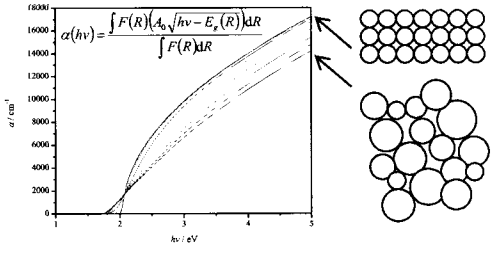

Band gap shifts due to size-distribution of nanoparticles in 3D assemblies built up by quantum dots in size-quantization regime.

New iodocuprates(I) with *N*-heterocyclic molecules as the cations

Jin-Jing Zhao, Xiao Zhang, Yan-Ning Wang, Hong-Li Jia, Jie-Hui Yu and Ji-Qing Xu

page 152

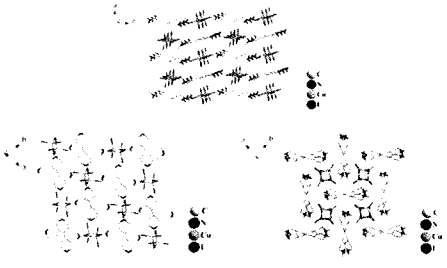

By employing hydrothermal *in situ* *N*-alkylation of bp/bpp with CH_3OH, three new organically templated iodocuprates(I) were obtained.

Effects of CO_2 activation on electrochemical performance of microporous carbons derived from poly(vinylidene fluoride)

Seul-Yi Lee and Soo-Jin Park

page 158

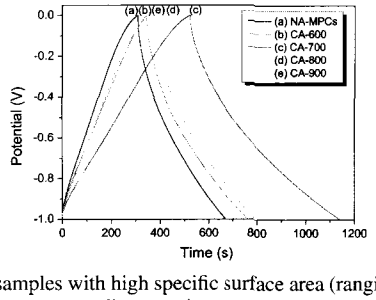

The A-MPC samples with high specific surface area (ranging from 1030 to 1082 m^2/g), corresponding to micropore sizes of 0.67 and 0.72 nm, and with the amount of oxygen-containing groups ranging from 3.2% to 4.4% have been evaluated as electrodes for EDLC applications.

Oxidation kinetics of aluminum diboride
Michael L. Whittaker, H.Y. Sohn and Raymond A. Cutler
page 163

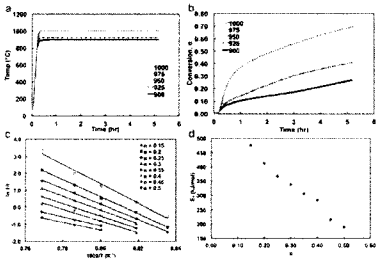

Isothermal kinetic data for AlB_2 in air, showing a constantly decreasing activation energy with increasing conversion. Model-free analysis allowed for the calculation of global kinetic parameters despite many simultaneous mechanisms occurring concurrently. (a) Time–temperature plots, (b) conversion as a function of time, (c) Arrhenius plots used to calculate activation energies, and (d) activation energy as a function of conversion.

Upcoversion performance improvement of $NaYF_4$:Yb, Er by Sn codoping: Enhanced emission intensity and reduced decay time
Han Yu, Wenbing Cao, Qingming Huang, En Ma, Xinqi Zhang and Jianchang Yu
page 170

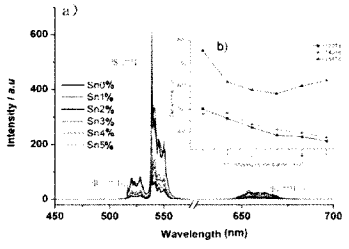

Variable-valenced Sn is introduced with Yb/Er into $NaFY_4$ to tune structure and local crystal field. Upconversion emission intensity of Er^{3+} was enhanced while decay time constant was decreased.

Two new polyoxometalate-based hybrids consisting of Keggin-type cluster modified by $\{Ag_4\}$ group
Xiaofang Zhao, Xiaowei Sun, Zhangang Han, Chuan Zhao, Haitao Yu and Xueliang Zhai
page 178

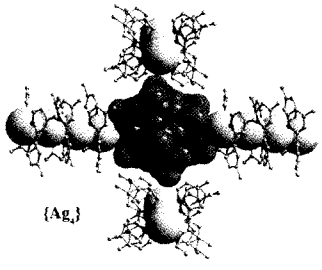

New polyoxometalate-based hybrids consisting of Keggin-type clusters modified by $\{Ag_4\}$ groups had been synthesized and characterized, and their photoluminescence properties were also discussed.

Distribution change of oxygen vacancies in layered perovskite type$(Sr, La)_{n+1}Fe_nO_{3n+1}$ (n=3)
Isao Kagomiya, Keigo Jimbo and Ken-ichi Kakimoto
page 184

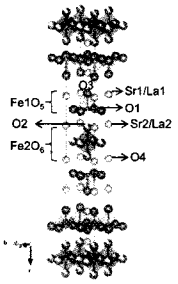

Crystal structure of $(Sr_{0.775}La_{0.225})_4Fe_3O_{10-\delta}$ (SLF4310) at 1000 °C.

Gas phase contributions to topochemical hydride reduction reactions
Yoji Kobayashi, Zhaofei Li, Kei Hirai, Cédric Tassel, François Loyer, Noriya Ichikawa, Naoyuki Abe, Takafumi Yamamoto, Yuichi Shimakawa, Kazuyoshi Yoshimura, Mikio Takano, Olivier J. Hernandez and Hiroshi Kageyama
page 190

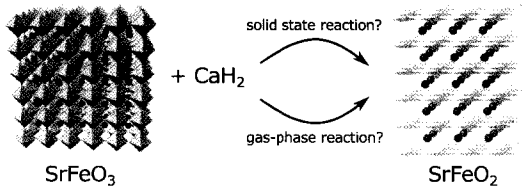

Topochemical reductions with hydrides: Solid state or gas phase reaction?

Sol–gel synthesis of MCM-41 silicas and selective vapor-phase modification of their surface
N.V. Roik and L.A. Belyakova
page 194

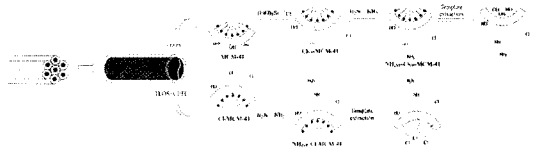

Sol–gel synthesis and postsynthetic chemical modification of template-filled MCM-41 and Cl-MCM-41 with (3-chloropropyl)triethoxysilane and 1,2-ethylenediamine in vapor phase.

Continued

Phase transition and conduction mechanism in $Pb_2Na_{0.8}R_{0.2}Nb_{4.8}Fe_{0.2}O_{15}$ material (R=rare earth)
M. Bouziane, M. Taibi and A. Boukhari
page 203

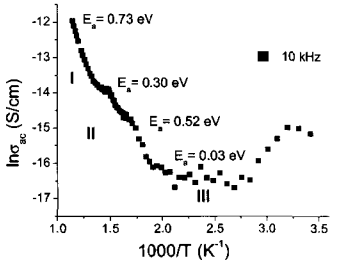

Thermal evolution of $\ln\sigma_{ac}$ of $Pb_2Na_{0.8}Eu_{0.2}Nb_{4.8}Fe_{0.2}O_{15}$ at selected frequencies.

NbF_5 and TaF_5: Assignment of ^{19}F NMR resonances and chemical bond analysis from GIPAW calculations
Mamata Biswal, Monique Body, Christophe Legein, Aymeric Sadoc and Florent Boucher
page 208

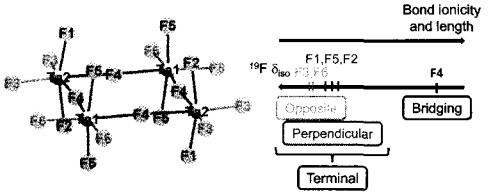

The complete assignment of the ^{19}F NMR lines of NbF_5 and TaF_5 allow establishing relationships between the ^{19}F δ_{iso} values, the nature of the fluorine atoms (bridging or terminal), the position of the terminal ones (opposite or perpendicular to the bridging ones), the fluorine charges, the ionicity and the length of the M–F bonds.

Rapid Communications

First-principles study on the structure, elastic properties, hardness and electronic structure of TMB_4 (TM=Cr, Re, Ru and Os) compounds
Y. Pan, W.T. Zheng, W.M. Guan, K.H. Zhang and X.F. Fan
page 29

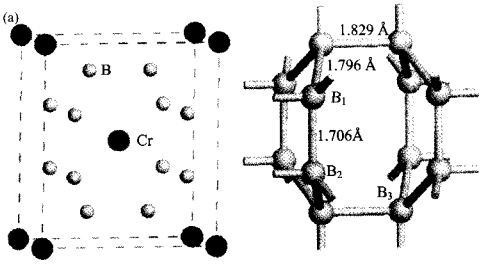

The first-principles calculations show that the intrinsic hardness of CrB_4 and ReB_4 are bigger than 40 GPa, which are the potential superhard materials due to the B–B bonds cage structure.